Second generation, high-power, fundamental mode large-orbit gyrotron experiments

K. Irwin, W. W. Destler, W. Lawson, and J. Rodgers
Electrical Engineering Department and Laboratory for Plasma Research, University of Maryland, College Park, Maryland 20742

E. P. Scannell and S. T. Spang
AAI Corporation, Hunt Valley, Maryland 21030

(Received 16 July 1990; accepted for publication 9 October 1990)

Experimental studies of a large-orbit gyrotron device operating at the fundamental of the cyclotron frequency have been conducted. Based on results of initial investigations at the University of Maryland a linear beam facility was retrofitted to produce rotating beams and a second experiment has been conducted. Experimental operation of this second device, aimed at the generation of rf radiation at ~ 650 MHz corresponding to a tangential intersection of the beam-waveguide dispersion curves is described.

I. INTRODUCTION

Large-orbit microwave devices have only recently been studied as high-power, low-frequency, rf sources.[1-3] Fundamentally, this relatively new class of microwave sources consists of an annular, rotating electron beam propagating through some resonant structure in the presence of an axial magnetic field. Typically, the device is identified according to the type of resonant circuit within which the microwave interaction occurs. If the beam travels within a magnetron-like multiresonator or smooth-walled waveguide, the device is most commonly referred to as a large-orbit gyrotron (LOG).[4-22] Whereas, if the beam interacts with azimuthally periodic magnetic fields, the designation of circulating free-electron laser[23-26] is more appropriate.

Experimental investigations of this class of device have shown it to operate efficiently at high harmonics of the electron-cyclotron frequency ($\ell\Omega_0$)[19,26] making it well-suited for high-frequency operation. The harmonic nature of the interaction enables substantial reductions in the requisite magnetic field for a given frequency. Largely ignored during this initial period of development, however, has been the low-frequency capability of this device. In fact, low-frequency LOG's driven by intense, relativistic electron beams offer several advantages over conventional, small-orbit gyrotrons operated at the same frequencies. Consider, for example, the LOG's annular Pierce-type diode versus the magnetron injection gun (MIG) used in the conventional gyrotron. The Pierce geometry, when associated with magnetic cusp injection, provides a higher maximum current capacity at the same time maintaining a substantially reduced beam width compared to the MIG.[27] Thus, current research at the University of Maryland has focussed on the performance of a smooth-walled LOG device driven by an annular, relativistic, cusp-injected beam. The desired resonance occurs between the fundamental ($\ell = 1$) harmonic of the beam-cyclotron frequency and the lowest order mode of the circular cylindrical guide, TE_{11}. Initial experiments,[1] which made use of an existing rotating beam facility (2 MeV, 2–3 kA, 5–15 ns) produced 500–1000 MW of rf at frequencies of 700 and 1200 MHz in agreement with theoretical predictions. Significant due to its relatively direct conversion to the TE_{10} rectangular waveguide mode, TE_{11} operation was verified using a microwave witness plate.

Various applications require lower frequency, longer pulse rf than could be obtained with the high-voltage rotating beam facility. Consequently, a linear beam device (the DRAGON accelerator)[28] was modified to generate large-orbit rotating beams. This paper details the initial testing of a high-power, low-frequency large-orbit microwave source driven by the lower voltage DRAGON accelerator. An overview of the linear theory used to predict LOG operation is presented in Sec. II. Following this, the design and operation of the second generation experiments are discussed in Sec. III. In Sec. IV, the work is summarized, conclusions are drawn, and future studies are suggested.

II. THEORETICAL DEVELOPMENT

Design parameters which establish microwave interaction at the appropriate frequencies are predicted using the tenuous beam formulation of the linear growth-rate formula.[10] Growth in the EM field is assumed to occur as a result of a resonant interaction between a thin, annular, rotating electron sheath and an empty cylindrical waveguide mode. Consider an electron beam of radius r_0 propagating axially through a circular cylindrical waveguide of radius r_w immersed in a uniform axial magnetic field, $B_0\hat{z}$. Produced via cusp injection,[29-32] the beam is assumed to be cold, displaying only axial ($c\beta_{z_0}$) and azimuthal ($c\beta_{\theta_0}$) velocity components. Further, it is assumed tenuous [$\delta(r - r_0)$], permitting the dc self fields to be neglected. Waveguide restrictions of axisymmetry and invariance to axial translations allow Fourier decomposition of the beam density perturbations to $e^{i(k_z z + \ell\theta - \omega t)}$ indicating that only the ℓth azimuthal harmonic exists. Based on this simplification, the total time derivative can be replaced by $-i\psi_l$ where ψ_l is given by

 0021-8979/91/020627-05$03.00

$$\psi_l = \omega - \omega_{\text{beam}},$$

and indicates the frequency deviation of the EM wave (ω) from the Doppler-shifted cyclotron harmonic associated with the beam density fluctuations

$$\omega_{\text{beam}} = \ell\Omega_0 + c\beta_{z_0}k_z,$$

where $\Omega_0 = eB_0/m_0\gamma_0$ and γ_0 is the relativistic mass factor.

Growth of the EM field is a result of the synchronous rotational interaction of a beam density perturbation and the EM wave, which implies $\psi_l \ll \Omega_0$. For the idealized beam model involved in this analysis, synchronism, hence maximum growth, occurs at intersections of the beam line with an empty cylindrical waveguide mode. The two points of resonant interaction are given by

$$c(k_z)_{\pm} = \gamma_{z_0}^2 \ell\Omega_0\beta_{z_0} \pm \gamma_{z_0}\sqrt{(\gamma_{z_0}\ell\Omega_0)^2 - (\zeta c)^2},$$

where $\gamma_{z_0}^{-2} = 1 - \beta_{z_0}^2$, $\zeta^2 = (\omega_c/c)^2$ and ω_c is the cutoff frequency for the mode of interest.

Continuing the analysis with $\psi_l = \omega_r + i\Gamma$ so that $\Gamma > 0$ denotes temporal growth, and assuming $\ell = 1$ and operation in vacuum, the normalized linear growth rates can be shown to be,[10] for TE waveguide modes,

$$\frac{\Gamma_{\text{TE}}}{\Omega_0} = \frac{\sqrt{3}}{2}\left(\frac{2\nu}{\gamma_0}\frac{(c/r_w)^2}{\Omega_0\omega}\right)^{1/3}\left|\frac{x_0 J_l'(x_0)}{\sqrt{1 - l^2/x_w^2}\,J_l(x_w)}\right|^{2/3}$$

and for TM modes

$$\frac{\Gamma_{\text{TM}}}{\Omega_*} = \frac{\sqrt{3}}{2}\left(\frac{2\nu}{\gamma_0}\frac{(c/r_w)^2}{\Omega_*\omega}\right)^{1/3}\left|\frac{J_l(x_0)}{J_l'(x_w)}\right|^{2/3},$$

where $\nu = eI/(4\pi\epsilon_0 c^3 m_0\beta_{z_0})$ is Budker's parameter, I is the beam current, $\Omega_* = ck_z - \omega\beta_{z_0}$, J_l is the Bessel function of the first kind of order ℓ, $x_w = x(r_w)$, $x_0 = x(r_0)$ and $x(r) = r(\omega^2/c^2 - k_z^2)^{1/2}$. The real part of ψ_l, which denotes a shift in the resonant frequency, is given by

$$\omega_r = \Gamma/\sqrt{3}$$

for both TE and TM modes.

III. SECOND GENERATION EXPERIMENTS

The DRAGON accelerator facility (500–800 kV, 140 kA, 100 ns) was used during the second phase of the fundamental mode LOG investigations (LOG II).[33] The linear growth rates, displayed in Fig. 1, were used to establish a viable design. The design parameters presented in Table I were selected to promote a microwave interaction at a single resonant frequency. Indicated on the dispersion relation for the LOG II design (Fig. 2) as a tangential intersection of the ($\ell = 1$) beam line and the TE_{11} mode, the appeal of this interaction over conventional two-point resonance is related to its anticipated advantages. The most significant of these are: (1) it displays the largest forward wave TE growth rate for a given azimuthal harmonic (ℓ), and (2) $v_{\text{group}} = v_{\text{phase}}$, indicating that the energy propagates along with the perturbation. Thus, the tangential intersection supports the strongest, most efficient, EM-beam interaction.

Designing for a tangential intersection is straightforward. Since $k_{z+} = k_{z-}$, two equations emerge from the quadratic form presented earlier. These equations can be used to solve for a grazing incidence beam radius

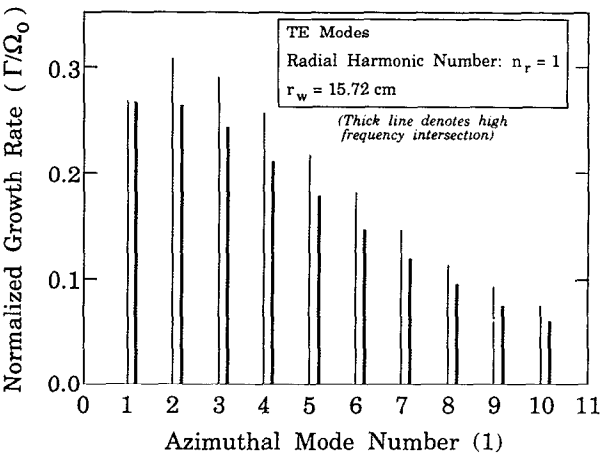

FIG. 1. Linear growth rates for the second generation experiments.

$$r_0|_{\text{grazing}} = \sqrt{(1/\omega_c^2) - (1/\Omega_c^2)},$$

where $\Omega_c = eB_0/m_0$ is the nonrelativistic cyclotron frequency and $\omega_c = c\zeta = \alpha_{ln}c/r_w$ is the cutoff frequency for the mode of interest, in which α_{ln} is the nth root of J_l'. Dependence on beam energy is implicit in the above expression according to the following relation developed during the unabridged form of the growth-rate analysis

$$\frac{r_0}{r_w} \leqslant \frac{l}{\{\alpha_{ln},\beta_{ln}\}}\frac{\gamma_0\beta_{\theta_0}}{\sqrt{1 + (\gamma_0\beta_{\theta_0})^2}},$$

in which $J_l(\beta_{ln}) = 0$ and the equality applies for the case of tangential intersection. Based on these considerations, the parameters of Table I, as indicated by the LOG II dispersion relation, were anticipated to promote a single 650 MHz resonant interaction.

The experimental apparatus constructed for the LOG II investigations, shown in Fig. 3, was essentially a scaled version of the earlier device. An annular slit in the anode, attached to the iron plate, allows the beam to penetrate through the cusp transition to the interaction region. Sandwiched between two oppositely energized sets of pancake coils, the iron plate is used to confine the radial magnetic

TABLE I. LOG II fundamental parameters.

Electron energy	750 keV
Axial magnetic field	450 Gauss
Beam radius	7.65 cm
Wall radius	15.716 cm
Cyclotron frequency	$2\pi\times 510$ MHz
$\alpha = \beta_{\theta_0}/\beta_{z_0}$	2.01
Cutoff frequency (TE_{11})	$2\pi\times 559$ MHz
Cutoff magnetic field	502 Gauss
Cutoff beam voltage	640 keV

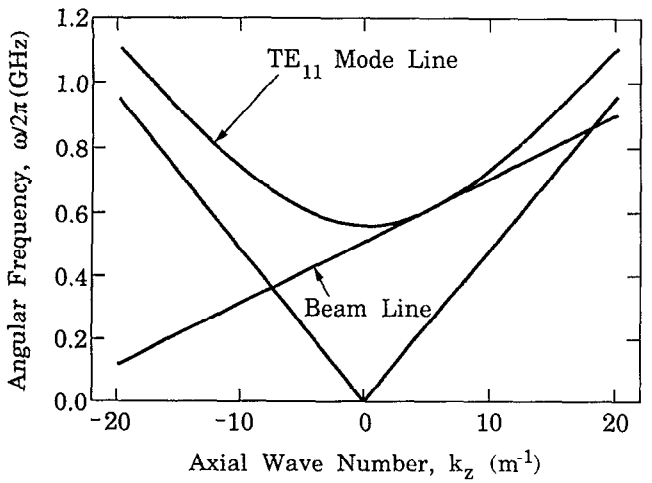

FIG. 2. Dispersion curves depicting the tangential beam-waveguide intersection at 650 MHz.

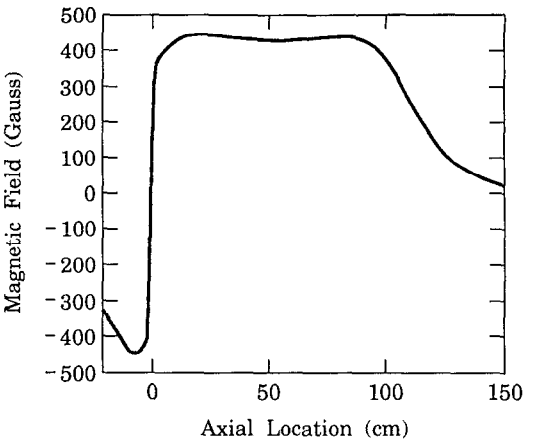

FIG. 4. Measured axial magnetic field profile, displaying the cusp transition and interaction regions.

flux. Two long solenoids downstream of the cusp transition provide for essentially adiabatic electron motion within interaction region. A typical axial magnetic field profile, displaying both the cusp and drift region fields is shown in Fig. 4. Because the DRAGON accelerator had never been used to accelerate rotating electron beams, tests were conducted first to examine diode and cusp performance, second to characterize the beam, and last to analyze the rf output.

A flat 560 kV, 80 ns pulse was obtained from the DRAGON accelerator by regulating the concentration of a sodium thiosulphate solution dummy load so that, together with the LOG II diode, the parallel combination established a matched load for DRAGON's $\sim 7\Omega$ pulse-forming line. A graphite cathode ($r_0 = 7.65$ cm) energized by the pulse was used to explosively emit an intense, annular electron beam. The voltage of the E-layer, though less than the 750 kV specified in the initial designs, was established as the maximum repeatable operating voltage due to limitations associated with the accelerator. Injected current was measured using a Faraday cup and regulated to ~ 1 kA by adjusting the AK gap to 0.875 in. During the microwave experiments, injected current was measured using a single-turn Rogowski coil, positioned on the downstream side of the iron plate and calibrated using Faraday cup data.

Beam quality was examined using a Čerenkov witness plate. The radiation produced as the electrons impact a 0.063-in.-thick polycarbonate disk was recorded on Polaroid 667 film through an open-shutter camera. Suitable beam quality several rotations downstream was observed for $V_0 = 560$ kV, $B_0 = 370$ G, as shown in Fig. 5.

The experimentally achieved dispersion relation is shown in Fig. 6. Notice the frequency of least separation of the $\ell = 1$ beam line and the TE_{11} waveguide mode near 650 MHz, which corresponds to the targeted resonance. Note further a second harmonic ($\ell = 2$) interaction with the

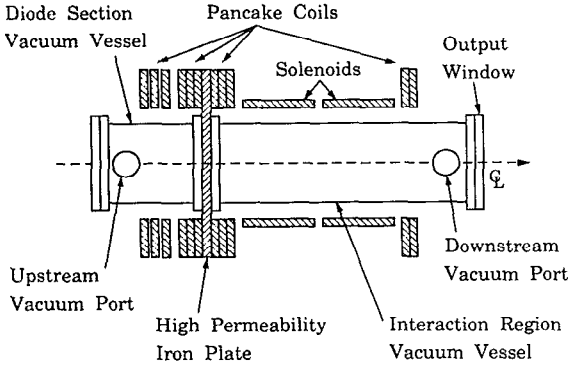

FIG. 3. The LOG II experimental apparatus.

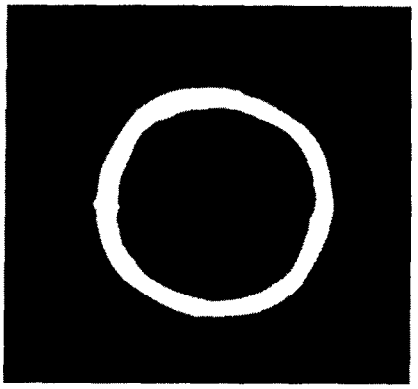

FIG. 5. Time-integrated photograph of rotating beam striking a graphite-covered polycarbonate witness plate 12.5 cm downstream of cusp transition ($B_0 = 370$ Gauss).

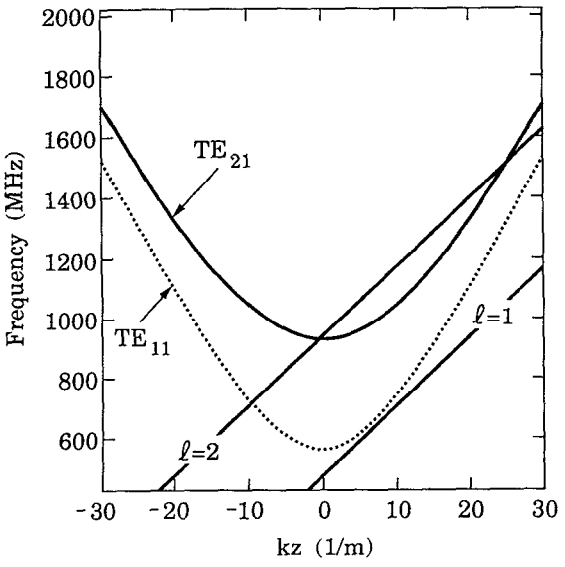

FIG. 6. Achieved dispersion relation for the second generation experiments displaying both the $\ell = 1$ and $\ell = 2$ resonances.

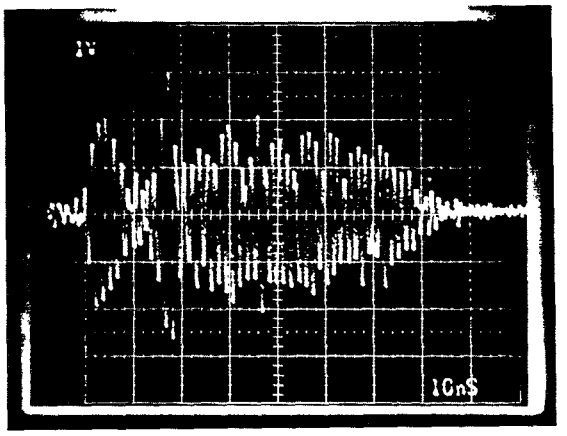

FIG. 8. Typical raw rf waveform acquired during the experiments.

TE_{21} mode for which resonances are expected at ~ 950 and ~ 1300 MHz.

At this point, power and spectral measurements were initiated. A survey of microwave power versus magnetic field indicated maximum power over the range $350 \leqslant B_0 \leqslant 370$ G, consistent with the level previously associated with optimal diode and cusp performance.

Spectral measurements were taken using the diagnostic arrangement displayed in Fig. 7. The WR-975 rectangular waveguide antenna was positioned at various azimuthal locations around a 1.7-m radius semicircle with center at the LOG II output window, on axis. The data collected in this

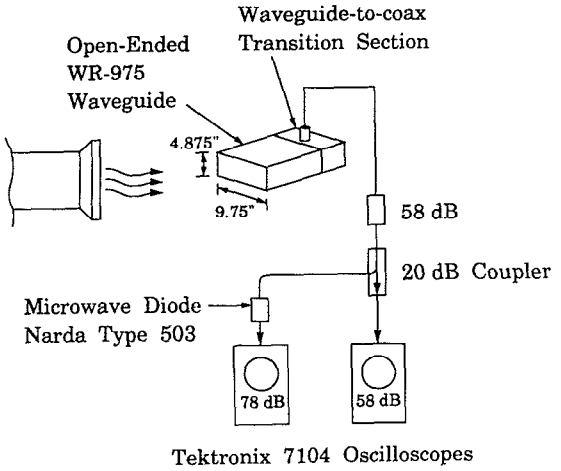

FIG. 7. Diagnostic setup used for power and spectral measurements.

survey indicated essentially pure 665-MHz rf signals directly on and far off ($\theta \geqslant 45°$) the system's central axis. From $\theta = 17°$ through 45°, a high-frequency component at ~ 1100 MHz was observed competing with the low-frequency signal. Based on the dispersion relation (Fig. 6) the low-frequency components are assumed to be produced through the desired $\ell = 1$ resonance, while the high-frequency signals are attributed to the second-harmonic interaction affected by beam velocity spread. The linear growth rate data, indicating the maximum forward wave growth rate for the TE_{21} mode, is consistent with this assessment. The off-axis variation in the received spectrum is evidence of the superposition of the radiation patterns of the lowest two TE modes, although experimental difficulties in separating the 1100 MHz signal from the 665 MHz output have prevented a more careful measurement of the radiation patterns of the two modes. Fourier analysis of a typical raw rf waveform, shown in Fig. 8, collected on axis ($\theta = 0°$) indicates, as shown in Fig. 9, a sharp peak at ~ 665 MHz. This value is consistent with the dispersion relation prediction for the $\ell = 1$ intersection.

For the power measurements, the rf radiation produced by the device was sampled using the same WR-975 receiving antenna as that used in the spectral determinations. The power incident over the cross section of the receiving guide was measured using a calibrated detector with operational range 0.3–3.0 GHz. Typical diode voltage and microwave detector output waveforms are shown in Fig. 10. Using the detector calibration curve, accounting for the line attenuation, and dividing by the effective aperture of the receiving antenna, intercepted power densities of 13 MW/m^2 peak and 2 MW/m^2 average were determined at a distance of 1.7 m from the LOG II output window, on axis. Performing the same off-axis survey done during the frequency measurements, essentially uniform power was observed over the spherical cap subtended by $\theta \leqslant 42.5°$, yielding $A_{\text{rad}} = 4.6$ m^2. Polarization tests performed at all angles confirm that equal power was observed in both polarizations, resulting in total

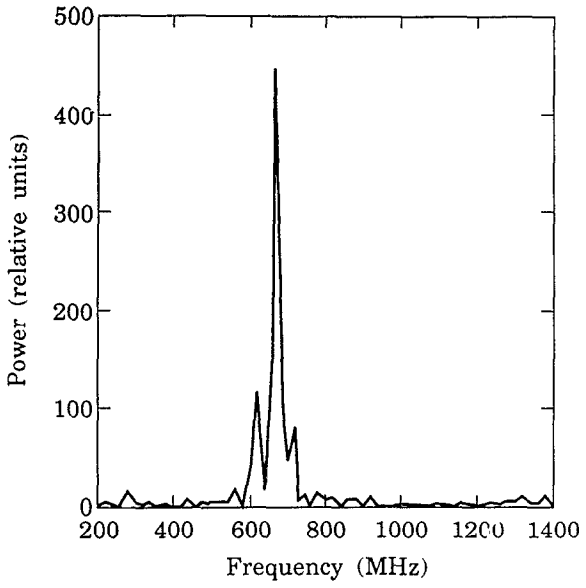

FIG. 9. Fourier analysis of the signal shown in Fig. 7.

power levels of 120 MW peak, and 20 MW averaged over the pulse. Based on Faraday cup data, $I_0 = 1.2$ kA from which beam ($P_0 = V_0 I_0 \cong 660$ MW) to microwave power efficiencies of 18% peak and 3% average are calculated.

IV. CONCLUSIONS

An existing linear beam device has been adapted to the production of cusp-injected, rotating electron beams. The attached smooth-walled LOG device, designed to operate at a single TE resonance, targeted $\ell = 1$ operation at ~650 MHz. Substantial deviations from the original design parameters, however, were required for successful operation of the device. The actual design was never fully realized, instead a weak, near grazing, fundamental mode resonance (650 MHz) together with a higher-frequency (1100 MHz), second harmonic interaction were observed. Peak and pulse-average powers of 120 MW and 20 MW were observed.

A number of potential future studies for this device are apparent. To promote the desired tangential intersection in the second generation device, either beam energy must be increased from ~600 keV to ~750 keV, or the cutoff frequency of the TE_{11} mode must be lowered. A dielectric liner, which could be used to accomplish this second possibility, by attenuating the off-axis fields, also promotes the dominance of the $\ell = 1$ interaction.

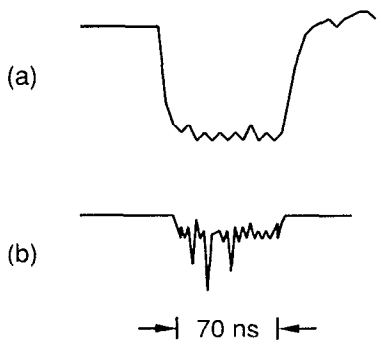

FIG. 10. Typical (a) diode voltage and (b) microwave detector output waveforms.

ACKNOWLEDGMENTS

It is an pleasure to thank J. Pyle for his assistance and technical expertise. The loan of the WR-975 waveguide antenna from Harry Diamond Laboratories is gratefully acknowledged, as is the aid of Dr. M. Fazio of Los Alamos National Laboratory in performing the spectral analysis of the raw rf waveform. This work was supported by the Maryland Industrial Partnerships program and by the AAI corporation.

[1] W. W. Destler, K. Irwin, W. Lawson, J. Rodgers, Z. Segalov, E. P. Scannell, and S. T. Spang, J. Appl. Phys. **66**, 4089 (1989).
[2] W. Namkung, J. Y. Choe, H. S. Uhm, and V. Ayres, in *1987 International Conference on Infrared and Millimeter Waves Conference Record*, edited by R. J. Temkin (IEEE, New York, 1987), p. 387.
[3] W. Namkung, in Proceedings of the O-E/Lase 1988, Symposium on Innovative Science and Technology, Los Angeles, 10–15 January 1988 (SPIE, Bellingham, WA), p. 104.
[4] R. J. Briggs and V. K. Neil, J. Nucl. Energy Part C **9**, 209 (1967).
[5] P. Sprangle, J. Appl. Phys. **47**, 2935 (1976).
[6] H. S. Uhm and R. C. Davidson, J. Appl. Phys. **49**, 593 (1978).
[7] Y. Y. Lau and L. R. Barnett, Int. J. Infrared Millimeter Waves **3**, 619 (1982).
[8] K. R. Chu and D. Dialetis, Int. J. Infrared Millimeter Waves **5**, 37 (1984).
[9] D. Chernin and Y. Y. Lau, Phys. Fluids **27**, 2319 (1984).
[10] W. Lawson and C. D. Striffler, Phys. Fluids **28**, 2868 (1985).
[11] W. Lawson and C. D. Striffler, Phys. Fluids **29**, 1682 (1986).
[12] W. Lawson and P. E. Latham, J. Appl. Phys. **61**, 519 (1987).
[13] W. W. Destler, D. W. Hudgings, M. J. Rhee, S. Kawasaki, and V. L. Granatstein, J. Appl. Phys. **48**, 3291 (1977).
[14] W. W. Destler, H. Romero, C. D. Striffler, R. L. Weiler, and W. Namkung, J. Appl. Phys. **52**, 2740 (1981).
[15] W. W. Destler, R. L. Weiler, and C. D. Striffler, Appl. Phys. Lett. **38**, 570 (1981).
[16] W. W. Destler, R. Kulkarni, C. D. Striffler, and R. L. Weiler, J. Appl. Phys. **54**, 4152 (1983).
[17] D. B. McDermott, N. C. Luhmann, Jr., P. S. Furuno, and A. Kupiszewski, Int. J. Infrared Millimeter Waves **4**, 639 (1983).
[18] W. Namkung, Phys. Fluids **27**, 329 (1984).
[19] W. Lawson, W. W. Destler, and C. D. Striffler, IEEE Trans. Plasma Sci. **PS-13**, 444 (1985).
[20] K. K. Tiong, S. P. Kuo, and P. E. Miller, in *1987 International Conference on Infrared and Millimeter Waves Conference Record*, edited by R. J. Temkin (IEEE, New York, 1987), p. 393.
[21] W. W. Destler, E. Chojnacki, R. F. Hoeberling, W. Lawson, A. Singh, and C. D. Striffler, IEEE Trans. Plasma Sci. **16**, 71 (1988).
[22] W. Lawson, J. Appl. Phys. **50**, 1477 (1987).
[23] G. Bekefi, R. E. Shefer, and W. W. Destler, Appl. Phys. Lett. **44**, 280 (1984).
[24] W. W. Destler, F. M. Aghamir, D. A. Boyd, G. Bekefi, R. E. Shefer, and Y. Z. Yin, Phys. Fluids **28**, 1962 (1985).
[25] E. Chojnacki and W. W. Destler, IEEE J. Quantum Electron. **QE-23**, 1605 (1987).
[26] E. Chojnacki, W. W. Destler, W. Lawson, and W. Namkung, J. Appl. Phys. **61**, 1268 (1987).
[27] W. Lawson, IEEE Trans. Plasma Sci. **16**, 290 (1988).
[28] A. Shpilman, Ma. thesis, University of Maryland (1983).
[29] M. J. Rhee and W. W. Destler, Phys. Fluids **17**, 1574 (1974).
[30] W. W. Destler, P. K. Misra, and M. J. Rhee, Phys. Fluids **18**, 1820 (1975).
[31] G. Schmidt, Phys. Fluids **5**, 994 (1962).
[32] J. G. Kalnins, H. Kim, and D. L. Nelson, IEEE Trans. **NS-18**, 473 (1971).
[33] K. Irwin, Ma. thesis, University of Maryland (1990).